The electronic structure of MgO nanotubes. An ab initio quantum mechanical investigation.

The electronic structure of MgO nanotubes. An ab initio quantum mechanical investigation.

Khaled E. El-Kelany,[1,*] Matteo Ferrabone,[2] Michel Rérat,[1] Philippe Carbonnière,[1] Claudio M. Zicovich-Wilson,[3] and Roberto Dovesi[2]

[1] *Equipe de Chimie Physique, IPREM UMR5254, Université de Pau et des Pays de l'Adour, 64000 Pau, France*

[2] *Dipartimento di Chimica IFM, Università di Torino and NIS -Nanostructured Interfaces and Surfaces - Centre of Excellence, http://www.nis.unito.it Via P. Giuria 7, 10125 Torino, Italy*

[3] *Facultad de Ciencias, Universidad Autnoma del Estado de Morelos, Av. Universidad, 1001, Col. Chamilpa, 62209 Cuernavaca (Morelos), Mexico*

(Dated: March 28, 2013)

Abstract

The structural, vibrational and response properties of the (n,0) and (m,m) MgO nanotubes are computed by using a gaussian type basis set, a hybrid functional (B3LYP) and the CRYSTAL09 code. Tubes in the range $6 \leq n \leq 140$ and $3 \leq m \leq 70$ have been considered, being $n = 2 * m$ the number of MgO units in the unit cell (so, the maximum number of atoms is 280). Tubes are built by rolling up the fully relaxed 2-dimensional conventional cell (2 MgO units, with oxygen atoms protruding from the Mg plane alternately up and down by 0.38 Å). The relative stability of the (n,0) with respect to the (m,m) family, the relaxation energy and equilibrium geometry, the band gap, the IR vibrational frequencies and intensities, and the electronic and ionic contributions to the polarizability are reported. All these properties are shown to converge smoothly to the monolayer values. Absence of negative vibrational frequencies confirms that the tubes have a stable structure. The parallel component of the polarizability $\alpha^{\parallel}$ converges very rapidly to the monolayer value, whereas $\alpha^{\perp}$ is still changing at n=140; however, when extrapolated to very large n values, it coincides with the monolayer value to within 1%. The electronic contribution to α is in all cases ($\alpha^{\parallel}$ and $\alpha^{\perp}$; $6 \leq n \leq 140$) smaller than the vibrational contribution by about a factor of three, at variance with respect to more covalent tubes such as the BN ones, for which the ratio between the two contributions is reversed.

Keywords: Nanotubes, MgO, polarizability components, electronic and ionic contributions, B3LYP hybrid functional, gaussian basis sets, CRYSTAL code

I. INTRODUCTION

Since their discovery,[1] carbon nanotubes (CNT) have attracted the attention of the scientific community for their unique electrical, mechanical and thermal properties.[2] Search for noncarbon nanotubes started very soon, at first in the domain of layered highly anisotropic phases such as hexagonal boron nitride and transition metal disulfides compounds that can also adopt cage-like structures such as fullerenes,[3–5] and then exploring isotropic inorganic compounds that can be "precursors" of nanomaterials in a large variety of morphological forms. Nowadays, big attention is paid to preparation of nanomaterials based on NaCl-like compounds, such as MgO. Solid MgO is known to be an inert material with a high melting point, consistent with strong ionic bonding, and a wide band gap of 7.8 eV.[6] Its substrate has been used for high-temperature superconductor (HTSC) thin-film coating applications worldwide. Properties of materials at a finite scale of length are often different from the corresponding bulk properties. For example, a pronounced covalent contribution to the ionic bonding exists in small MgO nanoparticles, whereas almost pure ionic bonds are typical for the bulk of this compound.[7–17] The atomic structures of small-sized MgO clusters have been investigated experimentally[7,18] and theoretically.[7–17] Mass spectroscopy experiments[18,19] indicate that small $(MgO)_3$ subunits are relatively stable. " Magic $(MgO)_i$ clusters" for $i = 2$, 4, 6, 9, 12, and 15 have been discovered by Ziemann and Castleman using laser-ionization time-of-flight mass spectrometry.[7]

In the present paper we investigate the properties of two families of MgO tubes, namely $(n,0)$ and (n,n). In both cases the coordination of cations and anions is 4, as in the monolayer, whereas it is 6 in the bulk. In the (n,n) case however cation rings alternate with anion rings, whereas in $(n,0)$ tubes oxygen and magnesium atoms are present in the same ring (see figure 1). The same scheme has been previously used for investigating (CNT)[20,21] imogolite[22], chrysotile[23], BNNT[24]. Recent improvements in the CRYSTAL09 code permit full use of symmetry (the point group contains $140 * 4 = 560$ symmetry operators for the $(140, 0)$ tube) so as to drastically reduce the computational cost. The total energy and its difference with respect to the MgO monolayer (l-MgO), the relaxation geometry and energy, the IR vibrational frequencies and intensities are investigated as a function of n. The polarizability of the tube (both parallel and perpendicular components, electronic and ionic contribution) is also explored, and it is shown to tend to the monolayer values as $n \to \infty$.

The structure of the paper is as follows: section II is devoted to the description of the method, section III presents the results whereas a few conclusions are drawn in section IV.

II. COMPUTATIONAL METHOD AND DETAILS

Calculations were performed by using the periodic *ab initio* CRYSTAL09 code[25], the hybrid B3LYP functional of the density functional theory (DFT)[26] and a Gaussian type basis set (a 8-511G* contraction for Mg,[27] and a 8-411G* set for O[28], where the exponents of the most diffuse valence shells were optimized). The DFT exchange-correlation contribution is evaluated by numerical integration over the unit cell volume. Radial and angular points of the integration grid are generated through Gauss-Legendre radial quadrature and Lebedev two-dimensional angular point distributions. A (99,1454) pruned grid (XXLGRID keyword in the CRYSTAL09 manual),[29] corresponding to 99 radial and 1454 angular points, was employed. The integration accuracy can be estimated by the error in the electronic charge per unit cell, $\Delta_e = 1.0 \times 10^{-3}|e|$ (out of a total of 2800 electrons for the (140,0) MgO nanotube). Other details on the grid generation and its influence on the accuracy and cost can be found in Ref. 30. Evaluation of the Coulomb and exact exchange infinite series is controlled by five parameters[29] (T_1, T_2, T_3, T_4, T_5), whose values are set to $T_1 = T_2 = T_3 = T_4 = \frac{1}{2}T_5 = T_I$. In this work we used $T_I = 10$ and a shrinking factor (the number of points along each reciprocal lattice vector at which the Fock matrix is diagonalized) $IS = 8$. The electronic polarizability is evaluated through the Coupled Perturbed Kohn-Sham (CPKS) scheme.[31,32] Convergence of the SCF zeroth-order energy and CPHF/CPKS iterations is controlled by the T_E and T_{CP} parameters, respectively. The SCF cycles are terminated when the difference between the values of the total energy (E) or polarizability (α) for two successive cycles is less than 10^{-T_E} Hartree or $10^{-T_{CP}}$ Bohr^3, respectively: here $T_E = 11$ and $T_{CP} = 4$ are used. Sometimes iterations produce large oscillations in the Fock/KS matrix, in which case these matrices were damped by mixing at the m and $m-1$ cycles with the FMIXING parameter[29] of 60%. Symmetry of the tubes (rototranslational and planes, both vertical and horizontal) is fully exploited in the calculation, so that, in spite of a high number of atoms in the tube unit cell (up to 280) and the use of an all-electrons basis set and a hybrid functional, the computational cost is low. For example, a full structure optimization (18 steps) on a local computing cluster with 12 cores (Intel Xeon X5660 2.8 GHZ) costs about two hours of elapsed time for

the $n = 100$ tube.

A. Geometry optimization

Fractional atomic coordinates and unit-cell parameters were optimized within a quasi-Newton scheme using analytic energy gradients combined with the BFGS algorithm for Hessian updating.[33–36] The two kinds of tubes have been rolled up (see the "NANOTUBE" keyword in the Nanotubes' tutorial at www.crystal.unito.it) starting from the primitive 2D cell (1 MgO units), and imposing the full rototranslational symmetry (560 operators for the (140,0) tube). After geometry optimization, the vibrational spectrum has been computed. The presence of imaginary frequencies in the spectrum indicates that the optimized structure is not a true global minimum. Symmetry has then been reduced in order to eliminate constraints and locate the correct equilibrium geometry. To this aim the normal coordinates corresponding to the imaginary frequencies have been explored looking for a new energy minimum. The vibrational frequencies obtained on the resulting structure are all positive. The very large relaxation taking place in the nanotubes is due to the fact that the 2D cell containing 1 MgO unit is not the most stable structure for the monolayer. A much more physical model for the MgO slab is obtained by considering a supercell of the 2D lattice containing 2 MgO units, as shown in figure 1. If this double 2D cell is optimized, the same kind of buckling observed in the nanotubes is reproduced in the monolayer. When the tubes are rolled up starting from this larger non planar 2D cell, the number of symmetry operators is half than starting from the planar layer (280 for the (140,0) tube, as only half of the cations and of the anions are symmetry related). All the frequencies are in this case positive, confirming that the equilibrium position is a real minimum. The effect of such relaxation is illustrated in figure 2. Open circles give the trend of the energy difference between the unbuckled nanotubes and the unbuckled planar slab. The full circles provide the same energy difference when the buckled structures are considered.

B. Frequencies and polarizability

The total static polarizability is determined as follows:

$$\alpha_0 = \alpha_e + \sum_j \frac{\overline{Z}_j^2}{\nu_j^2} \tag{1}$$

where α_e is the electronic (clamped ion) contribution. The vibrational (ionic) contribution is given, in the double harmonic approximation, by the second term on the right hand side. Frequencies were obtained by diagonalizing the dynamical matrix, found by numerical differentiation of the analytical energy gradients (see Ref. 37 for details). $\overline{Z}_j^2$ is a mass weighted effective mode Born charge and ν_j is the vibrational frequency of the mode j. Born charges were calculated using a Berry phase-like scheme[38,39]. For the largest tube ($n = 140$) there are more than 20 modes at less than 10 cm^{-1}; the Eckart conditions[40] are imposed in order to eliminate translational and rotational spurious contributions to the dynamic matrix.

III. RESULTS AND DISCUSSION

A. Bulk and monolayer

For comparison we report here bulk MgO and (001) monolayer properties. If planarity is imposed to the layer, the surface formation energy is 0.974 eV and the lattice parameter of the primitive cell (containing one Mg and one O atom/cell) shrinks from $a = 4.23$ Å (the bulk value; the experiment[41] is at 4.19 Å) to 2.80 Å (corresponding to 3.96 Å in a double cell). However this geometry is a saddle point rather than a minimum, as the negative value of one border-zone ($\vec{k} = (0.5, 0.5)$) frequency confirms (-129 cm^{-1}). This mode corresponds to the displacement of the two oxygen atoms in opposite directions along z. When a double cell is optimized the oxygen atoms move vertically by ±0.38 Å, the lattice parameter further reduces to 3.89 Å and the energy lowers by 0.035 eV/MgO. The bulk band gap (BG) is 7.4 eV (7.8 eV from experiment[42]); it increases to 9.65 eV in the relaxed monolayer. The triple-degenerate $F_{1\nu}$ transverse optical (TO) and longitudinal optical (LO) vibrational modes are at 384 cm^{-1} and 759 cm^{-1} (exp = 394 cm^{-1} and 724 cm^{-1}, respectively[41]); they split into two modes (A and E) with $\nu = 577$ cm^{-1} and 609 cm^{-1} for the planar slab and 572 cm^{-1}

and 621 cm^{-1} for the non planar one.

The calculated value of the bulk dielectric constant ϵ_e (electronic) is 2.48 to be compared to 2.38 from experiment[43]. The value of the static α_0 constant is 9.69 (9.83 from experiment[44]). The fully relaxed $\alpha^{\parallel}$ and $\alpha^{\perp}$ slab values are 2.258 and 0.811 for α_e and 7.082 and 1.761 $Å^3$ for α_0 (the corresponding numbers for the planar slab are 2.241, 0.756, 7.091 and 1.832 $Å^3$). Mulliken net charges in the bulk are ± 1.81 $|e|$ and the bond population is as small as $+0.004$ $|e|$, confirming the fully ionic nature of the Mg-O bond. In the slab the Mulliken net charges are slightly smaller (± 1.72 $|e|$) and the bond population slightly larger ($+0.027$ $|e|$), indicating the appearance of some degree of covalent character. The nanotube charge and bond population are very close to the values in the slab even at low n values (± 1.72 $|e|$ and $+0.026$ $|e|$, respectively, at n=12) and converge very rapidly to the slab limiting value. Born charges provide a measure of the polarizability of the system, and represent a more physical measure of the behaviour of the charge distribution. Their value (we report one third of the trace of the tensor) is 1.98 for the bulk, 1.66 for the monolayer and 1.51 for the (12,0) MgO nanotube, with a variation from the bulk to the (12,0) nanotube nearly five times larger than for the Mulliken charges.

B. Nanotubes: geometry and energy

Table I, first column, shows ($\bar{\Delta}$E), the energy difference between the (n,0) and the ($n/2$,$n/2$) tubes (see also figure 4, top). $\bar{\Delta}$E is as large as 16 mHa (0.435 eV) per MgO at n=12 (24 atoms) and decreases by two orders of magnitude to 0.158 mHa (0.0043 eV) per MgO at n=140 (280 atoms). There are two possible reasons for the larger stability of the (n,0) tubes with respect to the ($n/2$,$n/2$) ones: a) a different pattern of the fourfold coordination of both cations and anions (for the ($n/2$,$n/2$) tubes the four neighbors of Mg belong to different rings, whereas for (n,0) two of the neighbors are on the same ring, as shown in figure 1, b) the lower radius (and the higher strain) of ($n/2$,$n/2$) tubes with respect to (n,0), as shown in figure 3. In order to separate these two effects, $\bar{\Delta}$E has also been reported as a function of the tube radius (we used R_{Mg} for the comparison); the results are shown in figure 4, bottom. It turns out that the separation of the two curves reduces drastically; (n,0) tubes are, however, more stable than the (m,m) tubes, the difference tending to zero for very large tubes.

The second column in table I provides the relaxation energy δE of the (n,0) tubes, i.e. the energy difference between the equilibrium structure of the tube and the value obtained by rigidly rolling up the equilibrium monolayer. For the smallest tube it is as large as 33.6 mHa (0.914 eV) per MgO unit, then it decreases rapidly (see figure 5). At $n = 100$ δE is negligible (4 μHa or 0.0001 eV, about four orders of magnitude smaller than for $n = 6$). The third column provides ΔE, the energy difference between the tube and the monolayer. Also ΔE becomes negligible (35 μHa or 0.00095 eV) at n larger than 100. It should be noticed that the very regular behaviour of both curves, shown in figure 5, documents the high numerical accuracy of the code; the ΔE trend also implies that the same accuracy is obtained when treating systems of different dimensionality (1D and 2D). Columns R_u, R_{Mg} and R_O provide a measure of geometrical relaxation, that for the smallest tubes is very important, as shown by figure 3. There are two types of O atoms, "inside" and "outside" the Mg ring (as was for the slab, with one oxygen above and one below the Mg plane). For small radii all atoms tend to move outwards, in order to reduce the strain; in (12,0), the Mg radius increases by 0.11 Å whereas one anion (O outside) moves farther away by as much as 0.53 Å, in order to reduce short range repulsion, which is no more compensated by the strong electrostatic field as in the bulk. The oxygen moving "inside" reduces its radius by 0.23 Å. At larger radii (the figure reports data for (24,0) and (12,12)) relaxation is nearly negligible, and the two oxygen radii are already at $\pm$0.38 Å with respect to the Mg radius, as in the slab they are at $\pm$0.38 Å from the Mg monolayer.

C. Nanotubes: band gap and polarizability

The bandgap (BG) shows good convergence to the slab indirect gap value of 9.65 eV: it is 9.02 eV at $n = 6$ (this tube is very strained), increases to 9.55 eV at $n = 12$ and reaches 9.60 eV at $n = 48$. The last six columns in table I report the values of the parallel and perpendicular polarizability of the (n,0) tubes as a function of n (see also figure 6). The electronic uncoupled contribution (often indicated as Sum Over States - SOS -) is first reported; it corresponds to the situation in which the effect of the applied field on the charge distribution is not taken into account (in other words the unperturbed charge distribution interacts with the field). Then, the fully coupled polarizability is given, as resulting from the CPKS-SCF scheme.[45] It is interesting to note that the coupling (resulting from the dif-

ference between α_e and α_{SOS}) increases by about 7% the parallel value, and decreases by more than 31% the perpendicular value at $n = 6$. At the other extreme ($n = 140$) the correction remains essentially the same for $\alpha^{\parallel}$ (7%), and reduces to about 15% for $\alpha^{\perp}$. The two components ($\alpha^{\parallel}$ and $\alpha^{\perp}$) have about the same value at the SOS level, whereas for the fully coupled case $\alpha^{\parallel}$ is about two times larger than $\alpha^{\perp}$ at $n = 6$; this ratio decreases to 1.5 at $n = 140$. In the last line of the table the values for the monolayer are shown: the asymptotic value for the tubes, obtained by fitting the data from $n = 24$ to $n = 140$ are also reported. The asymptotic (∞) and the monolayer values differ by less than 1% in all cases. Finally, the vibrational contribution to the polarizability (α_{vib}) is also shown, as obtained from a frequency calculation ($\alpha_{vib} = \alpha_0$ - α_e, table I). The vibrational contribution is larger by a factor 1.4 than the electronic one for $\alpha^{\perp}$ at $n = 6$, but increases much faster than the latter along the series: at $n = 140$ the electronic contribution is only 37% of the total. For the parallel contribution the situation is slightly different: the vibrational contribution is about two times the electronic one at n=6, and this ratio remains about constant up to $n = 140$. The parallel component of α_0 increases along the series by about 0.8 $\mathring{A}^3$, to be compared to 1.5 $\mathring{A}^3$ for the perpendicular component. Also for the vibrational contribution the extrapolated value $\alpha(n \to \infty)$ is extremely close to the monolayer limit.

It is interesting to analyze where the vibrational contribution comes from. For all tubes there are only four IR active modes (whose symmetry is *A, E1, E2*, and *E3*). They are obviously the only ones that contribute to the polarizability. The A mode describes a motion that contributes to polarization along the tube axis (direction x in our orientation), whereas the twofold degenerate modes E contribute to the polarization in the other two directions (y and z, equivalent by symmetry). The wavenumbers and intensities are reported in table II and shown in figure 7 (in the latter only the results from n=24 are shown, to better identify the limiting values). In order to be able to extrapolate also the individual contributions to polarizability to the infinite radius limit, we performed two additional calculations for the (160,0) and (180,0) tubes (the latter contains 360 atoms). Graphical animation of the vibrational modes is provided as supplementary information on CRYSTAL's website (http://www.crystal.unito.it/prtfreq/jmol.html). The A mode corresponds to the opposite displacements of Mg and O atoms along the x-direction (the periodic direction). The corresponding vibrational frequency tends, in the infinite radius limit, to the one of the degenerate E modes of the monolayer. This mode contributes to the parallel polarizability

α_{xx} of the tube which, in turn, corresponds in the $n \to \infty$ limit to the parallel component of the monolayer α_{XX}. Table II shows that for the largest tubes the frequency and intensity coincide with the monolayer values. The twofold degenerate *E1* mode is similar to the *A* mode since Mg and O atoms move in opposite directions. Whereas in the *A* mode the displacement takes place along the periodic x-direction, in the *E1* mode the displacement is parallel to the circumference of the tube. This mode corresponds to the other component of the degenerate mode *E* of the monolayer, as confirmed by the trends of frequencies and intensities provided in table II. This mode contributes to the transverse polarizability of the nanotubes $\alpha_{yy} = \alpha_{zz}$, which in the $n \to \infty$ limit corresponds to half of the parallel polarizability of the slab $\alpha_{YY}/2$. The *E2* mode involves opposite displacements of Mg and O atoms along the direction which is perpendicular to the circumference of the tube. This mode is equivalent to the out of plane non degenerate mode of the monolayer. At the $n \to \infty$ limit the contribution of the *E2* mode to the transverse α_{zz} (α_{yy}) polarizability of the tube tends to half the perpendicular component α_{ZZ} of the slab ($\alpha_{zz} = \alpha_{yy} = 0.53$ Å^3 for n=180, while $\alpha_{ZZ}/2 = (1.761 - 0.811)/2 = 0.48$ Å^3). The *E3* mode is similar to the *E1* mode since the displacements of Mg and O atoms are opposite and parallel to the circumference of the tube. The only difference is that neighboring rows (rings) of atoms are moving in phase in *E1* while in *E3* they are moving in antiphase. In the slab this mode corresponds to a phonon in a point of the First Brillouin Zone different from Γ. For this reason in the $n \to \infty$ limit the contribution of this mode to the polarizability is vanishing. In all cases, as shown in table II and figure 7, the asymptotic values for frequencies, intensities and contribution to the polarizability coincide with high accuracy with the monolayer values.

It is interesting to compare the total polarizability of the MgO tube with the one of the more covalent BN case, for tubes of about the same radius. At n=60, the numbers to be compared with the 60 entry of our table I are 4.59 Å^3 (electronic contribution) and 7.15 Å^3 (total) for $\alpha^{\parallel}$ of BN, and 2.32 Å^3 and 3.17 Å^3 for $\alpha^{\perp}$ of BN[24]. The electronic contribution is then about twice larger for BN than for MgO, whereas the total α_0 of BN is about the same as in MgO, indicating that the vibrational contribution is much larger for MgO that for BN. The reason is simple: looking just at the largest contribution to polarizability and considering the limiting case of the slab, the BN frequency is larger than the MgO one (836 and 621 cm^{-1}, respectively; remember that the frequency appears squared to the denominator in the formula defining the polarizability) and the intensity (that appears in the numerator) much

smaller (13.06 km/mol for BN and 91 for MgO).

IV. CONCLUSIONS

In the present study the structural, vibrational and response properties of the MgO (n,0) and (m,m) nanotube families have been investigated. The (n,0) tubes have been shown to be more stable than the (m,m) ones; the energy difference decreases when the radius increases and both families tend to the monolayer case (described by a cell containing two MgO units, the two oxygen atoms being displaced above and below the Mg plane) regularly. Tubes are shown to be stable structure (all vibrational frequencies are positive). Both the electronic and the ionic (vibrational) contributions to the polarizability have been evaluated and compared to the ones of the monolayer. The components parallel to the tube axis converge very rapidly to the monolayer asymptotic value, whereas convergence of the perpendicular component is much slower. The electronic contribution to the polarizability is smaller than the vibrational one, indicating that these tubes are characterized by IR active modes with very low frequencies. Overall, this study shows that the properties of tubes as large as (140,0), that contains 280 atoms in the unit cell and has a radius not too far from the ones of technological interest (30 - 100 nm),[46] can be accurately simulated with a rich *all electron* basis set and adopting a sophisticated functional, such as the *hybrid* B3LYP.

Acknowledgements

The authors acknowledge the CINECA Award No. HP10BLSOR4-2012 for the availability of high performance computing resources and support, and mexican CONACyT for finantial support through project CB-2012-1 178853. El-Kelany also acknowledges the egyptian government for supporting a grant to do this work at the Université de Pau et des Pays de l'Adour in France.

* Chemistry Department, Faculty of Science, Minia University, Minia 61519, Egypt

[1] S. Ijima, Nature **354**, 96 (1991).

[2] M. U. Kahaly and U. V. Waghmare, J. Nanoscience and Nanotechnology **7**, 1787 (2007).

[3] P. J. F. Harris, *Carbon Nanotubes and related Structures: New Materials for the twenty-First Century* (Cambridge University Press, 1999).

[4] A. L. Ivanovskii, Russ. Chem. Rev. **71**, 203 (2002).

[5] R. Tenne and C. N. R. Rao, Phil. Trans. R. Soc. Lond. A **362**, 2099 (2004).

[6] S. H. Tamboli, R. B. Patil, S. V. Kamat, V. Puri, and R. K. Puri, J. Alloys Compd. **477**, 855 (2009).

[7] P. J. Ziemann, J. Chem. Phys. **94**, 718 (1991).

[8] T. M. Kohler, H. P. Gail, and E. Seldlmayr, Astron. Astrophys. **320**, 553 (1997).

[9] S. Moukouri and C. Noguera, Z. Phys. D: At., Mol. Clusters **24**, 71 (1992).

[10] S. Moukouri and C. Noguera, Z. Phys. D: At., Mol. Clusters **27**, 79 (1993).

[11] M. J. Malliavin and C. Coudary, J. Chem. Phys. **106**, 2323 (1997).

[12] C. Roberts and R. L. Johnston, Phys. Chem. Chem. Phys. **3**, 5024 (2001).

[13] J. M. Recio, R. L. Pandey, A. Ayuela, and A. B. Kunz, J. Chem. Phys. **98**, 4783 (1993).

[14] E. de la Puente, A. Aguado, A. Ayuela, and J. M. Lopez, Phys. Rev. B **56**, 7607 (1997).

[15] M. Wilson, J. Chem. Phys. **101**, 4917 (1997).

[16] S. Veliah, R. Pandey, Y. S. Li, J. M. Newsam, and B. Vessal, Chem. Phys. Lett. **235**, 53 (1995).

[17] F. Calvo, Phys. Rev. B **67**, 161403 (2003).

[18] W. A. Saunders, Phys. Rev. B **37**, 6583 (1988).

[19] W. A. Saunders, Phys. D: At., Mol. Clusters **12**, 601 (1989).

[20] Y. Noel, P. D'Arco, R. Demichelis, C. M. Zicovich-Wilson, and R. Dovesi, J. Comp. Chem. **31**, 855 (2010).

[21] R. Demichelis, Y. Noel, P. D'Arco, M. Rérat, C. M. Zicovich-Wilson, and R. Dovesi, J. Phys. Chem. **115**, 8876 (2011).

[22] R. Demichelis, Y. Noel, P. D'Arco, L. Maschion, R. Orlando, and R. Dovesi, J. Mater. Chem. **20**, 10417 (2010).

[23] P. D'Arco, Y. Noel, R. Demichelis, and R. Dovesi, J. Chem. Phys. **131** (2009).

[24] M. Ferrabone, B. Kirtman, M. Rérat, and R. Dovesi, Phys. Rev. B **83**, 235421 (2011).

[25] R. Dovesi, R. Orlando, B. Civalleri, C. Roetti, V. R. Saunders, and C. M. Zicovich-Wilson, Z. Kristallogr. **220**, 571 (2005).

[26] A. D. Becke, J. Chem. Phys. **98**, 5648 (1993).

[27] L. Valenzano, Y. Noel, R. Orlando, C. M. Zicovich-Wilson, M. Ferrero, and R. Dovesi, Theor. Chem. Acc. pp. DOI 10.1007/s00214–006–0213–2 (2006).

[28] F. Cora, Mol. Phys. **103**, 2483 (2005).

[29] R. Dovesi, V. R. Saunders, C. Roetti, R. Orlando, C. M. Zicovich-Wilson, F. Pascale, B. Civalleri, K. Doll, N. M. Harrison, I. J. Bush, et al., *CRYSTAL 2009 User's Manual* (University of Torino, Torino, 2009).

[30] M. Prencipe, F. Pascale, C. Zicovich-Wilson, V. Saunders, R. Orlando, and R. Dovesi, Phys. Chem. Min. **31**, 559 (2004).

[31] M. Ferrero, M. Rérat, R. Orlando, and R. Dovesi, J. Comp. Chem. **29**, 1450 (2008).

[32] M. Ferrero, M. Rérat, R. Orlando, and R. Dovesi, J. Chem. Phys. **128**, 014110 (2008).

[33] C. G. Broyden, J. Inst. Math. Appl. **6**, 76 (1970).

[34] R. Fletcher, Comput. J. **13**, 317 (1970).

[35] D. Goldfarb, Math. Comput. **24**, 23 (1970).

[36] D. F. Shanno, Math. Comput. **24**, 647 (1970).

[37] F. Pascale, C. M. Zicovich-Wilson, R. Orlando, C. Roetti, P. Ugliengo, and R. Dovesi, J. Phys. Chem. B **109**, 6146 (2005).

[38] R. Resta, Rev. Mod. Phys. **66**, 809 (1994).

[39] R. D. King-Smith and D. Vanderbilt, Phys. Rev. B **49**, 5828 (1994).

[40] C. Eckart, Phys. Rev. **47**, 552 (1935).

[41] O. L. Anderson and P. Andreatch, J. Am. Ceram. Soc. **49**, 404 (1966).

[42] R. C. Whited, C. J. Flaten, and W. C. Walker, Solid State Commun. **13**, 1903 (1973).

[43] E. D. Palik, *Handbook of Optical Constants of Solids* (London: Academic Press, 1991).

[44] J. Fontanella, C. Andeen, and D. Schuele, J. Appl. Phys. **45**, 2852 (1974).

[45] M. Ferrero, M. Rérat, R. Orlando, R. Dovesi, and I. J. Bush, J. Of Physics: Conference Series **117**, 012016 (2008).

[46] Y. B. Li, Y. Bando, D. Golberg, and Z. W. Liu, Appl. Phys. Lett. **83**, 999 (2003).

Figures

FIG. 1: The optimized geometry of MgO systems of different dimensionality: bulk ((a), 3D); primitive planar (unbuckled) and conventional non planar (buckled) cell of the monolayer ((b) and (c), 2D); (12,0) and (12,12) nanotubes, ((d) and (e), 1D).

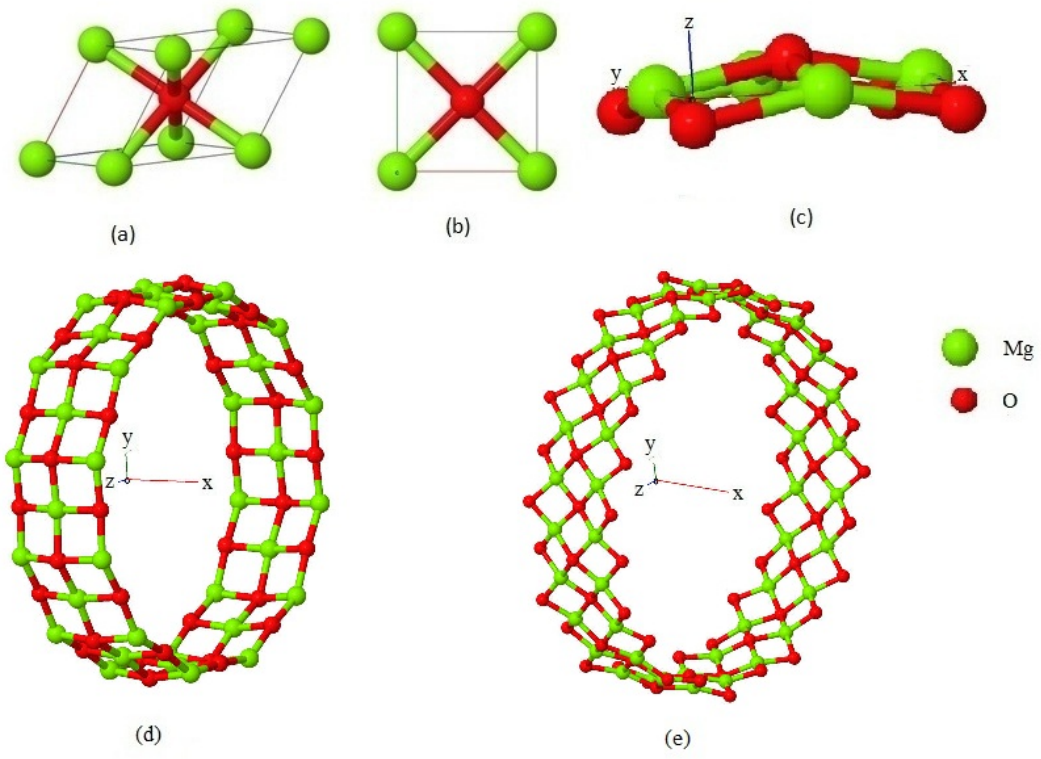

FIG. 2: Energy difference ΔE in mHa (10^{-3} Hartree) between the (n,0) nanotubes and the planar (unbuckled, open circle) and non planar (buckled, filled circles) monolayer of MgO. The zero of the energy corresponds to the non planar (conventional, double) cell. The energy of the primitive planar cell, containing 1 MgO units is 1.302 mHa (0.035 eV) higher. When all the oxygens are forced to be symmetry related (and then to have the same radial distance from the tube axis) the large radius limit is the planar slab. When oxygens are allowed to relax in opposite directions the tube energy tends to the relaxed monolayer, in which the oxygen atoms are protruding by ± 0.38 Å.

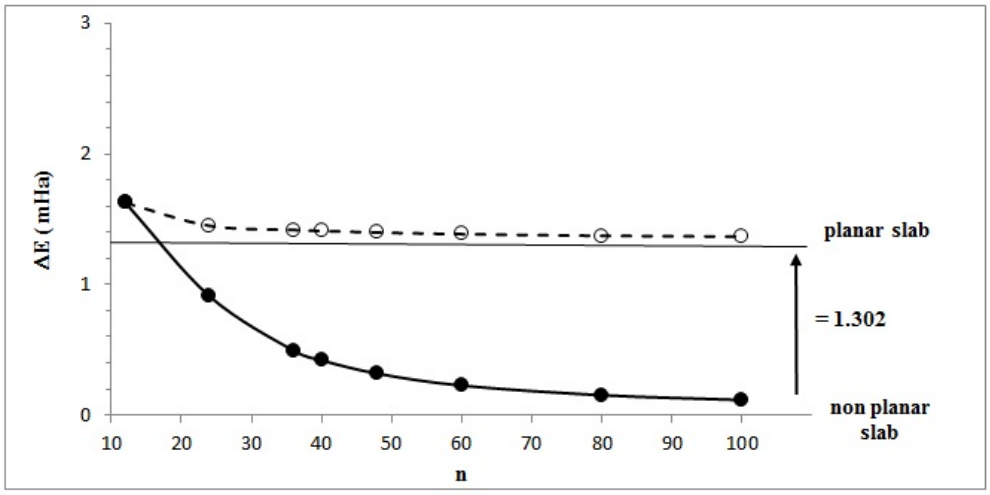

FIG. 3: The unrelaxed and relaxed distances (in Å) of Mg and O atoms from the tube axis for $(12,0)$, $(6,6)$, $(24,0)$ and $(12,12)$ tubes.

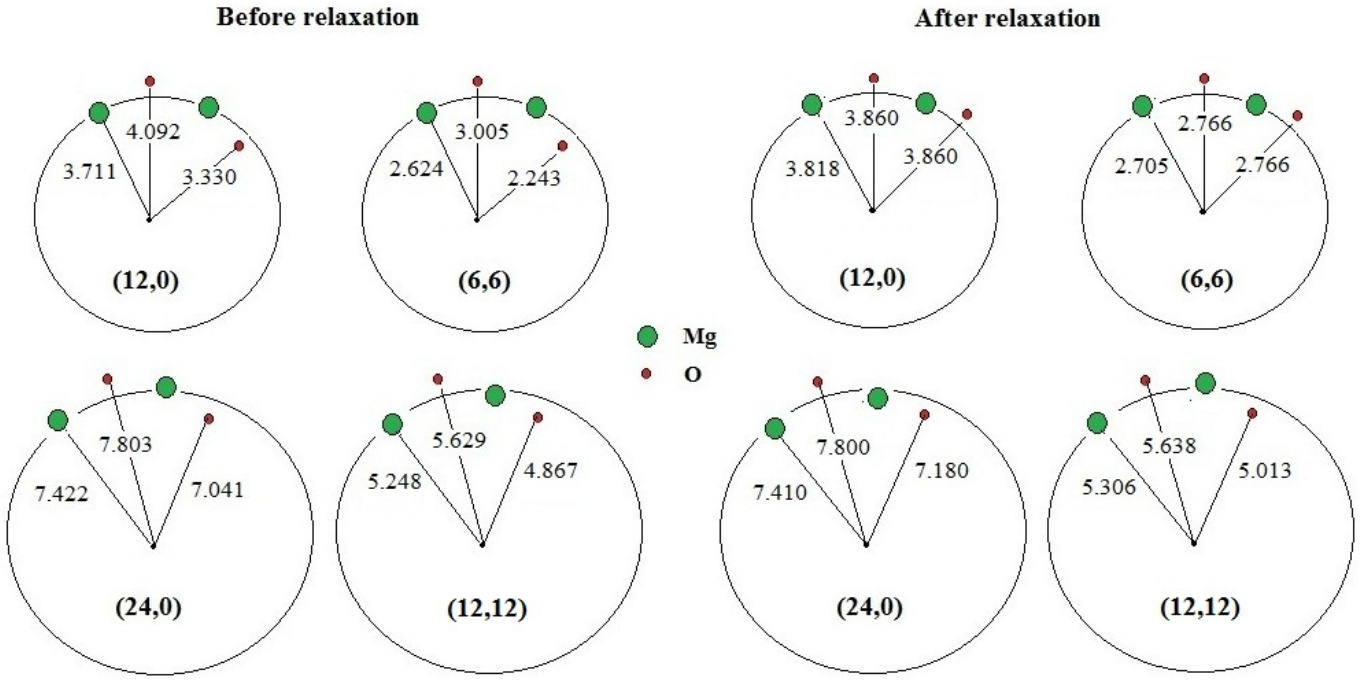

FIG. 4: Energy difference ΔE in mHa per MgO units with respect to the slab for the $(n, 0)$ (open circles) and $(n/2, n/2)$ (filled circles) tubes as a function of n (top). In the bottom figure the same energy difference is plotted as a function of the tube radius.

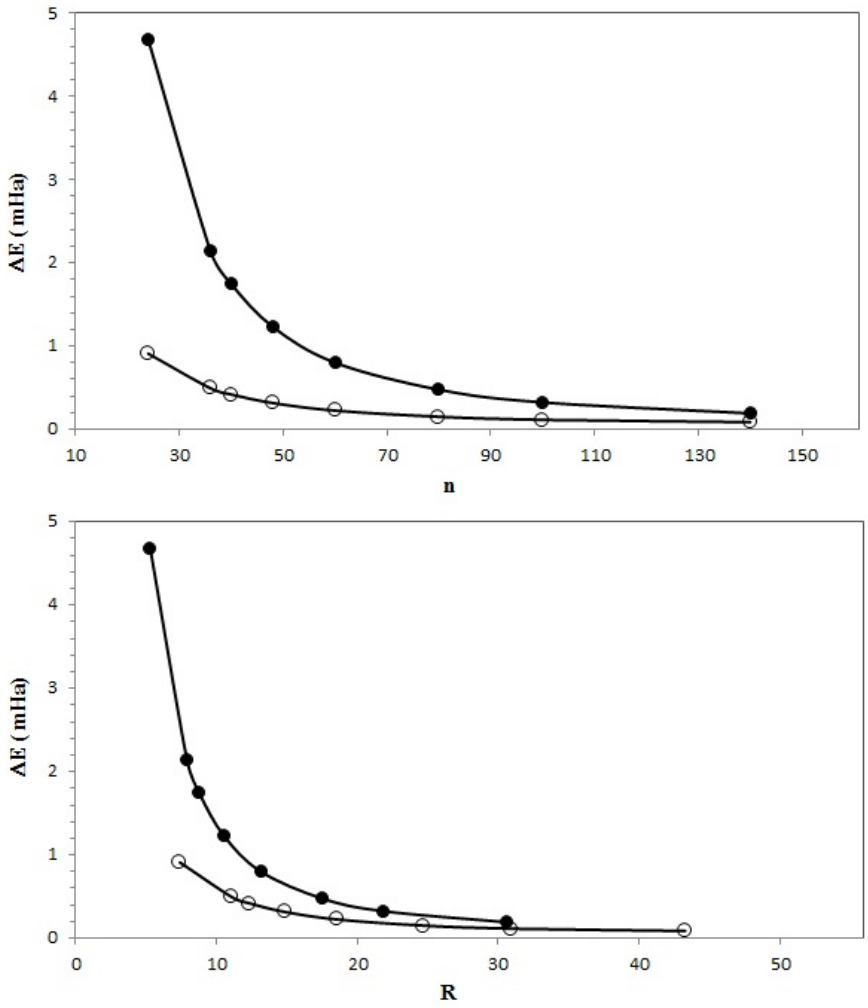

FIG. 5: Relaxation energy δE and energy difference ΔE between the relaxed $(n, 0)$ nanotube and the relaxed monolayer as a function of n. Energies are in mHa per MgO unit.

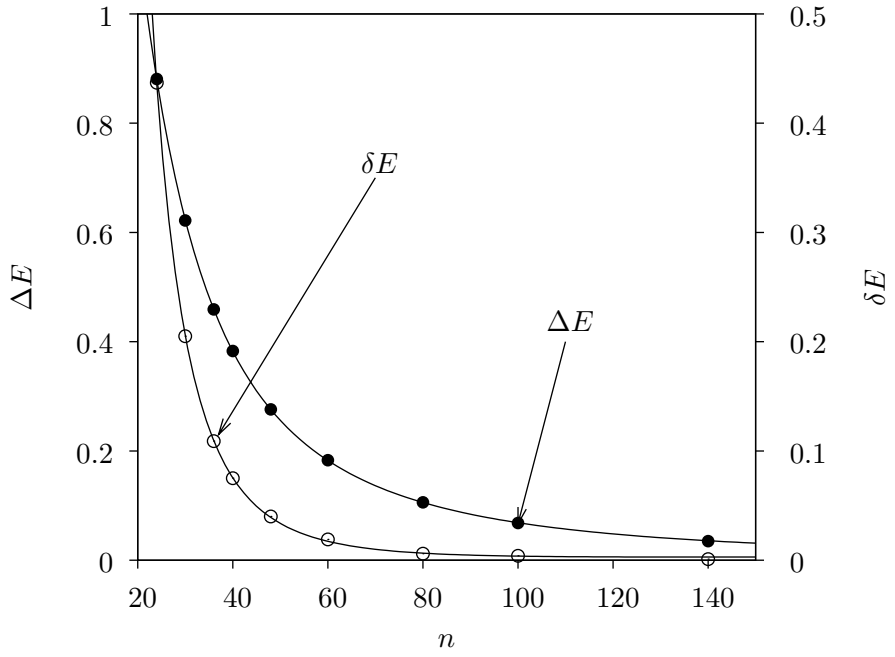

FIG. 6: The longitudinal $\alpha^{\parallel}$ and transverse $\alpha^{\perp}$ polarizability of (n,0) MgO nanotubes as a function of the nanotube size n. The electronic Uncoupled (or SOS: Sum Over States) α_{SOS}, the electronic Coupled α_e and the vibrational α_{vib} contributions are reported. Values are in Å^3 per MgO unit. The fitting function $\alpha = a + \frac{b}{n} + \frac{c}{n^2} + \frac{d}{n^3}$ has been used.

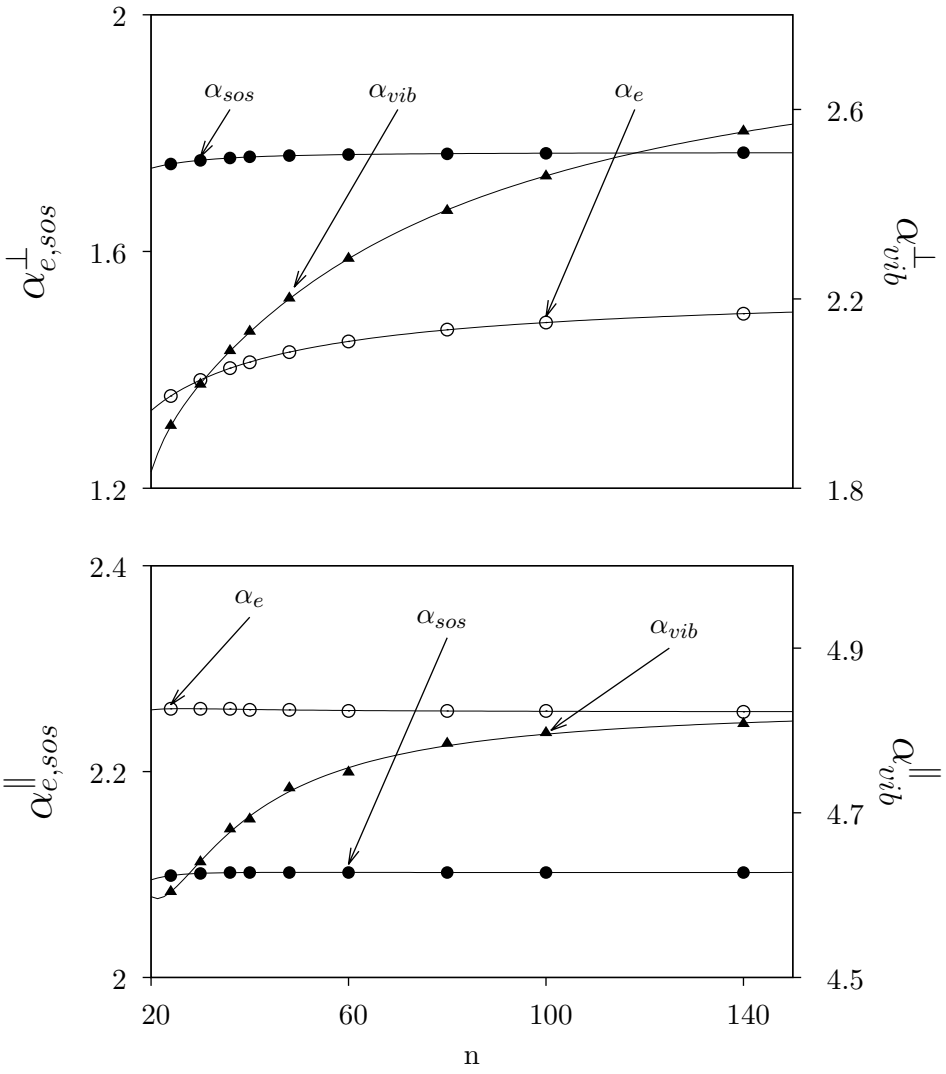

FIG. 7: Frequencies (ν) and intensities ($\mathcal{I}$) for the IR active modes of the (n,0) nanotubes as a function of n. The mode symmetry is indicated. The right scale in the frequency and intensity figures represents the data of the *E3* mode, and the left scale corresponds to the data for the other three modes *A, E1, E2*. Values are in cm^{-1} for frequency ν and km/mol for the intensity ($\mathcal{I}$).

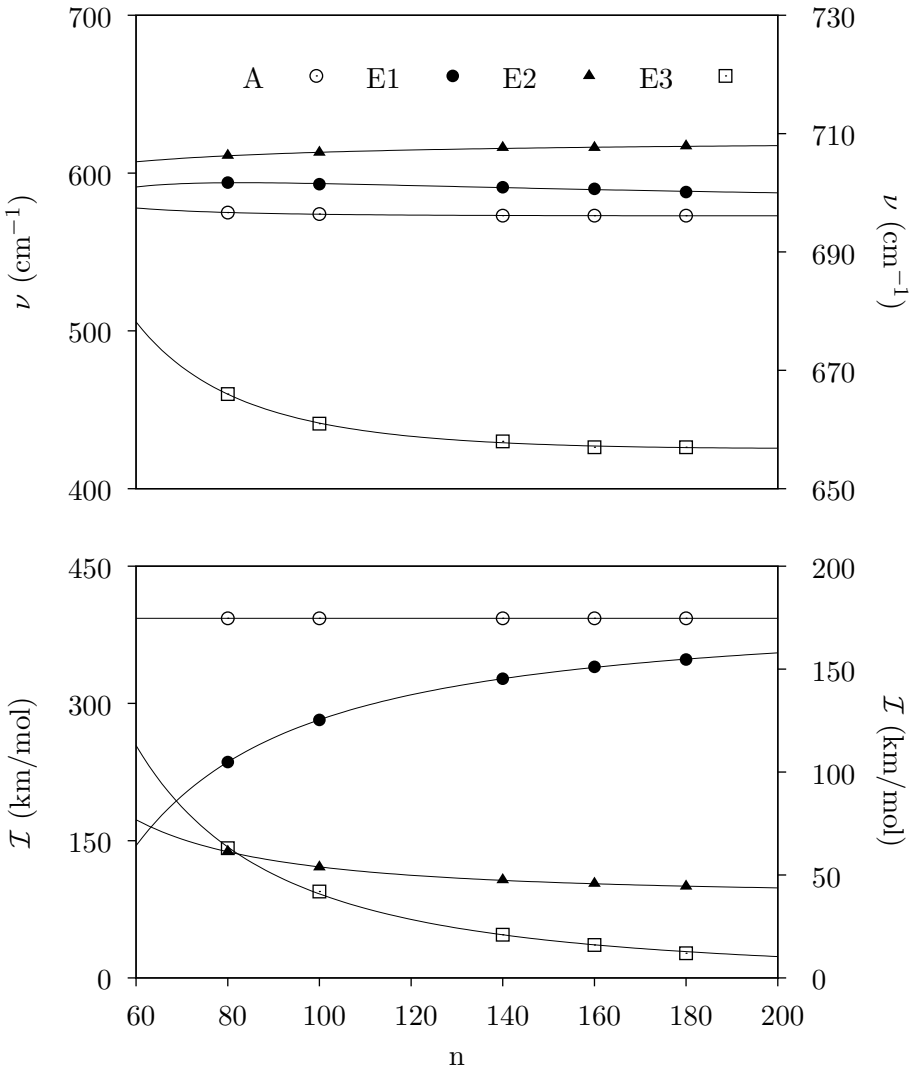

Tables

								$\alpha^{\parallel}$			$\alpha^{\perp}$		
n	$\bar{\Delta}$E	δE	ΔE	R_u	R_{Mg}	R_O	BG	α^e_{SOS}	α^e	α^0	α^e_{SOS}	α^e	α^0
6		33601	4568	1.86	1.98	2.06	9.02	2.134	2.300	6.239	1.803	1.236	2.951
12	15664	4489	1646	3.71	3.82	3.86	9.55	2.088	2.259	6.873	1.746	1.272	2.905
24	3801	437	881	7.42	7.41	7.18	9.56	2.099	2.261	6.865	1.748	1.356	3.287
30		205	622	9.28	9.26	8.99	9.58	2.101	2.261	6.900	1.754	1.383	3.402
36	1684	109	459	11.13	11.11	10.81	9.59	2.102	2.261	6.940	1.758	1.403	3.493
40	1364	75	383	12.37	12.35	12.04	9.59	2.102	2.260	6.953	1.760	1.413	3.544
48	956	40	276	14.84	14.82	14.49	9.60	2.102	2.260	6.990	1.762	1.430	3.632
60	619	19	183	18.56	18.54	18.19	9.61	2.102	2.259	7.009	1.764	1.448	3.733
80	372	6	106	24.74	24.73	24.37	9.62	2.102	2.259	7.043	1.765	1.468	3.853
100	257	4	68	30.93	30.91	30.55	9.62	2.102	2.259	7.056	1.766	1.480	3.939
140	158	1	35	43.29	43.28	42.91	9.63	2.102	2.258	7.066	1.767	1.495	4.049
∞		0	0				9.66	2.102	2.258	7.084	1.767	1.536	4.376
Layer$*$											1.767	1.535	4.422
Layer		0	0				9.65	2.101	2.258	7.082	1.432	0.811	1.761

TABLE I: Calculated properties of the (n,0) series of MgO nanotubes and of the monolayer (l-MgO). $\bar{\Delta}$E, δE and ΔE are the energy difference between the (n,0) tube and the corresponding ($n/2$,$n/2$) one (they have the same number of atoms), the relaxation energy for the rolled configuration and the energy difference between the relaxed tube and l-MgO, respectively. Values reported are in μHa per MgO unit. R_u is the unrelaxed radius (in Å) of the Mg cations (the anions O are at R_u±0.38); R_{Mg} and R_O are the same distances after relaxation (R_O refers to the "inner" oxygen, see text and figure 3). The radius of the oxygen atom "outside" the tube (at R_u + 0.38 before relaxation) remains essentially unaltered. BG is the band gap in eV. $\alpha^{\parallel}$ and $\alpha^{\perp}$ are the longitudinal and transverse components of the electronic α_e, and static α_0 polarizabilities per MgO unit (in $\mathring{A}^3$). The unrelaxed (sum over states) α_{SOS} values are also reported. The *Layer*$*$ row gives the average of the monolayer perpendicular polarizabilities per MgO unit using the relation $\alpha^{\perp}_n = \frac{1}{2}(\alpha^{\perp}_l + \alpha^{\parallel}_l)$ (l stands for layer, n is the label of the tube) which should be equal to the large radius limit (∞ row) of the transverse nanotube polarizability.

	$Frequency(\nu)$				$Intensity(\mathcal{I})$			
n	A	$E1$	$E2$	$E3$	A	$E1$	$E2$	$E3$
6	637	636	420	716	397	256	31	0
12	591	684	520	685	401	260	70	0
24	589	572	591	707	397	2	220	150
30	586	580	594	699	396	10	233	142
36	582	585	598	690	395	39	224	133
40	581	587	600	686	395	61	215	126
48	579	591	604	679	394	106	195	112
60	577	593	607	672	394	165	168	91
80	575	594	611	666	393	236	138	63
100	574	593	613	661	393	282	121	42
140	573	591	616	658	393	327	107	21
160	573	590	616	657	393	340	103	16
180	573	588	617	657	393	348	100	12
∞	572	574	621	656	393	401	90	0
Layer	572		621	654	786		91	0
	E		A	E'	E		A	E'

TABLE II: The IR active vibrational frequencies and intensities for the (n,0) series of MgO nanotubes and double cell monolayer (l-MgO). The extrapolated values are obtained by fitting the data from n=80 to n=180 with the function $f(n) = a + \frac{b}{n} + \frac{c}{n^2}$. The last line reports the double cell monolayer values. The tube modes A and *E1* modes of the tube correspond to the two components of the degenerated mode E of the slab. Whereas the degenerate *E2* and *E3* modes tend to the nondegenerate A and the degenerate E' modes of the monolayer, respectively. The intensity of the A and *E1* modes of the tube tends to $\frac{E_{slab}}{2} = \frac{786}{2} = 393$. Values reported are in cm^{-1} for the frequency and $\mathrm{km.mol}^{-1}$ for the intensity.